

Differentiating sharp phase transitions from mixed states in neutron stars

Jonas P. Pereira,^{1,*} Michał Bejger,^{2,1} J. Leszek Zdunik,¹ and Paweł Haensel¹

¹*Nicolaus Copernicus Astronomical Center, Polish Academy of Sciences, Bartycka 18, 00-716, Warsaw, Poland*

²*INFN Sezione di Ferrara, Via Saragat 1, 44122 Ferrara, Italy*

(Dated: January 5, 2022)

The internal composition of neutron stars is still an open issue in astrophysics. Their innermost regions are impervious to light propagation and gravitational waves mostly carry global aspects of stars, meaning that only indirect inferences of their interiors could be obtained. Here we estimate the observational accuracy and discuss ways to differentiate a mixed phase/state from a sharp phase transition region in a hybrid star by means of some electromagnetic and gravitational wave observables. We show that different transition constructions lead to similar sequences of stellar configurations due to their shared thermodynamic properties. In the most optimistic case - a strong quark-hadron density jump phase transition - radius and mass observations require fractional uncertainties smaller than 1 – 2% to differentiate mixed states from sharp phase transitions. For tidal deformations, relative uncertainties should be smaller than 5 – 10%. However, for masses around the onset of stable quark cores, relative tidal deformation changes associated with strong sharp phase transitions and mixed states connecting the two pure phases could be much larger (up to around 20 – 30%). If one compares purely hadronic stars (masses below their phase transition thresholds) with those having mixed states, relative tidal deformation and radius differences might be even more pronounced (roughly up to 50% and 5%, respectively). All the above suggests that 2.5- and 3rd generation gravitational wave detectors and near-term electromagnetic missions may be able to start assessing some aspects of phase transitions in neutron stars. Finally, we briefly discuss other observables that may also be relevant for such probes.

I. INTRODUCTION

It has long been hypothesized that neutron stars (NSs) contain exotic phases of matter, which are possible to exist solely due to unique conditions - density and pressure, particle fractions - present in their interiors [1]. The change from “normal” (nucleonic) matter to “exotic” matter (e.g. deconfined quarks) is thought to occur through a phase transition (or, in more general terms, state transition) process. Its detailed structure - sharp first order between the two pure phases or via a mixed state of the two phases - is still an open issue [2, 3], due to the complexity of direct quantum chromodynamics (QCD) calculations [4], or the lack of direct experimental observations of dense matter at high chemical potentials and low temperatures. The above clearly shows that the most promising laboratories for studying superdense matter aspects are NSs [5–8]. In general, a state transition between distinct phases of matter results in a *softening* of the pressure-density relation in the equation of state (EOS), which in turn results in more compact NSs (in terms of stellar parameters, this is quantified by larger values of the compactness parameter GM/Rc^2 , with M denoting the gravitational mass, and R the stellar radius), and a lower maximum mass M_{\max} than in the case of stars without state transitions, due to transitional deficit in pressure increase related to the softening. While a direct access to the interiors of NS is impossible, one can draw conclusions from astrophysical measurements of the stellar mass M and radius R with the use of

electromagnetic observables (see, e.g., [9–13]), as well as the tidal deformabilities Λ_i of the components of a binary system during its last orbits before the merger by means of gravitational wave (GW) signals ([14–20], see also [21] for a review), due to their dependence on the EOS; hence, one can expect potentially measurable imprints of dense-matter state transitions on these NS observables. For recent reviews on the dense-matter state transitions in NSs, see e.g., [22, 23].

In this work we *assume* that the state transition to exotic phases is realized in nature. We then discuss two types of state transitions: via a sharp boundary between pure phases (“density jump” phase transition), and a transition through a “mixed phases” (mixed state) region. Under the theoretical viewpoint, a macroscopically smoother phase transition (leading to the presence of an intermediate state—mixed phase/state) in a star—besides a sharp phase transition—is thermodynamically possible. Indeed, pasta phases [24, 25] for dense matter, where nuclei exist in non-spherical shapes, could be present in the bottom layer of an NS crust. In addition, there is plenty of room in models for hybrid stars where third families of NSs [26–30] are very distinct from purely hadronic stars, meaning that it would make observational sense to contrast a sharp transition with one having an intermediate state.

Specifically, in this article we will study EOSs exhibiting either a sharp phase transition or a mixed-state transition region, but otherwise possessing the same low-density part (a “nucleonic matter crust and outer core”) and high-density part (an “exotic core”), i.e., we will study the state transition *masquerade problem*, similar to the one first discussed in [31]. Using these EOSs we will

* jpereira@camk.edu.pl

study the importance of the presence of destabilisation of stellar configurations after the state transition (the so-called strong phase transition [32]) and study the observational accuracy needed to discriminate between the types of constructions (sharp vs mixed state) from the point of view of astrophysical observations of M , R and Λ , using current and planned observing infrastructure. Given that in terms of EOSs the two above-mentioned constructions would only differentiate in a finite region of their pressure-density planes, one would expect only a given range of macroscopic observables to evidence them. They should be associated with central pressures (chemical potentials) between the ones marking the appearance of the mixed state and when a quark phase becomes significant inside the star. We show with numerical examples and analytically that the above is exactly the case.

On the macroscopic level relevant for NSs, the mixed state of dense matter is electrically neutral. However, on the microscopic scale, the space there is filled with structures of normal and exotic phases of opposite electric charges [33, 34]. The Coulomb force is balanced out by the surface tension between the two phases [33]. Generally, the volume fraction occupied by the exotic phase grows with pressure, from zero at the top of the mixed state layer, to one at the bottom of it. The thickness of the mixed state layer is maximal for a surface tension going to zero and vanishes for a surface tension exceeding a critical value: then, the transition to the exotic phase is a sharp one. In view of the unavoidably large uncertainties plaguing the theory of dense matter in NS cores at supranuclear densities, one can only hope to shed light on the actual state of dense matter there via confronting theoretical dense matter models with forthcoming measurements of M , R , and Λ .

An interesting argument in favor of a phase transition at intermediate densities (3–4 ρ_{sat} , $\rho_{\text{sat}} = 2.7 \times 10^{14} \text{g cm}^{-3}$) may be derived from the precise measurement of the thickness of the neutron skin of ^{208}Pb (see [35] and references therein). The skin thickness being larger than anticipated requires a stiffer EOS of neutron matter at $\rho \lesssim \rho_{\text{sat}}$ [35]. If smoothly continued to intermediate supranuclear densities, relevant for NSs of masses around $1.4M_{\odot}$, this new EOS is too stiff to be reconciled with measured values of R and Λ , which require a softer EOS in this density region. This softening, followed by a stiffening at large densities—to allow for $2M_{\odot}$ NSs—is missing in the smooth EOSs based on ^{208}Pb skin measurements. According to [35], the tension between the two EOSs might indicate a phase transition at intermediate densities, relevant for NSs but irrelevant for ^{208}Pb .

In the near future, it will be possible to constrain masses and radii of stars with uncertainties of a few percent (see, e.g., [36, 37]). Uncertainties around 5–10% for tidal deformabilities will also be possible with third generation gravitational-wave detectors due their larger sensitivities (see, e.g., [38] and references therein). Therefore, the high precision associated with these observables justify their use to start differentiating sharp first or-

der phase transitions from smoother ones in NSs. We do not directly focus on stability issues associated with the mixed state. For an analysis in this direction, see [28]. Stability should be easily identified from the $M(R)$ sequences with the configurations to the right(left) of their maxima(minima); in general, $\partial M/\partial \rho_c \geq 0$, where ρ_c is the central density, see, e.g., [39] and references therein. Studies on the stability of rotating hybrid stars with mixed states and sharp phase transitions indicate that rotation does not change the global property of the (non)existence of the second branch of stable configurations [40].

The article is composed as follows: in Sect. II we present the simple, parametric models of the EOSs, used as an input to the Tolman-Oppenheimer-Volkoff (TOV) equations [41, 42], to produce sequences of M , R and Λ as functions of central pressure P and chemical potential μ . In Sect. III we study the sequences of configurations composed of EOSs which exhibit either “sharp” or “mixed” state transitions, i.e. diverging only in a specific well-defined region of pressure P –baryon chemical potential μ . We discuss how this feature impacts the $M(R)$ and $M(\Lambda)$ sequences, as well as the value of the maximum mass M_{max} , and assess the regions of astrophysical parameters, for which the “sharp” and “mixed” state transitions result in potentially observable differences (a state-transition *masquerade problem*). Section IV contains a discussion of the results from the point of view of a current and planned capabilities of the EM missions (NICER [43], Athena [44], eXTP [36, 37]) and the GW detectors (Advanced LIGO [45], Advanced Virgo [46], KAGRA [47], NEMO [48], Einstein Telescope [49], Cosmic Explorer [50]) in terms of measurements errors. Section V contains a relevant discussion, conclusions and an outlook. Section VI gives a detailed summary of our analysis.

II. PARAMETRIC MODELS OF THE EOS

The mixed phase/state in a hybrid star can be approximated in a variety of ways. Here, in Sect. II A, we present the construction put forth by [51] (for further applications, see [52]). Their main idea is to build on the Maxwell’s construction (sharp phase transition) and phenomenologically take into account certain properties of other (microscopic) mixed state constructions. In Sect. II B we present a simple sharp/mixed state transition based on the use of relativistic polytropes ([53]).

A. Mixed state construction of Abgaryan *et al.* 2018

We denote by μ_0 the baryon chemical potential at the quark-hadron phase transition coming from the Maxwell construction. One expects the presence of a mixed state to increase the phase transition pressure P à la Maxwell,

$P_0 \equiv P(\mu_0)$. The reason for that is the larger density of the mixed state with respect to the base of the hadron phase. The relative increase of pressure may be assumed to be given, as motivated by first principle constructions, and will be denoted by Δ_p . For the connection of Δ_p with microscopic parameters of the pasta phase, see [30]. In addition, assume that the pressure in the mixed state, P_m , in the simplest case is given by (parabolic expansion)

$$P_m(\mu) = (1 + \Delta_p)P_0 + \alpha_1(\mu - \mu_0) + \alpha_2(\mu - \mu_0)^2, \quad (1)$$

where α_1 and α_2 are free parameters to be found by demanding certain thermodynamic constraints. In particular, we impose the continuity of the mixed state pressure and its first derivative with respect to the baryon chemical potential (baryon number) at the hadronic ($\mu = \mu_h$) and quark ($\mu = \mu_q$) interfaces:

$$P_m(\mu_h) = P_h(\mu_h), \quad P_m(\mu_q) = P_q(\mu_q) \quad (2)$$

and

$$n_m(\mu_h) = n_h(\mu_h), \quad n_m(\mu_q) = n_q(\mu_q), \quad (3)$$

with μ_h and μ_q free adjustable quantities, P_h the hadronic EOS and P_q the quark EOS. Put in the above way, given a Δ_p , one has a system of four equations (2, 3) to four unknowns ($\mu_h, \mu_q, \alpha_1, \alpha_2$) to solve, and its solution should be unique. Obviously, the physically relevant solution should present $\mu_h < \mu_0 < \mu_q$. After solving the TOV equations for a given central density, one can find the extension of the mixed state by means of the knowledge of μ_h and μ_q . In addition, the continuity of the baryon number density at both borders of the mixed state implies that the energy density is also continuous there for hadronic and quark barotropic EOSs.

The speed of sound, c_s , on the other hand, is in general discontinuous at the hadronic and quark borders for the model given by Eq. (1). The reason is simply because it involves a second derivative of the pressure (with respect to μ), which is not guaranteed to be continuous at the borders of the mixed state for the parabolic mixed state construction. With the above prescription, it is not controllable and causality should be checked a posteriori. Given the causality of the speed of sound for both hadronic and quark phases and the expected EOS softening due to the mixed state, one would expect c_s^2 to also be causal there.

B. Mixed state polytropic EOSs

Here we put forth an effective, parametric multipolytrope model for both the sharp and mixed state transitions. Basic intensive thermodynamic properties of relativistic polytropes [53] are defined as:

$$\begin{aligned} P(n) &= Kn^\gamma, \\ \rho(n) &= n\varepsilon + \frac{P}{\gamma - 1}, \\ \mu(P) &= \varepsilon + \frac{\gamma}{\gamma - 1} \frac{P}{n}, \end{aligned} \quad (4)$$

where P is the pressure, ρ the mass-energy density, μ the chemical potential, ε the energy per baryon at $P = 0$ in a given phase, K is the polytropic ‘‘pressure’’ coefficient, and γ is called the adiabatic index. Pressure and energy-density are functions of the baryon number n , but later we will focus on the direct relation between the chemical potential and the pressure, $\mu(P)$.¹ A sharp phase transition may be defined as a ‘‘Maxwell construction’’ at the first order phase transition point (P_0, n_0) between two polytropes $(K_1, \gamma_1, \varepsilon_1)$ and $(K_2, \gamma_2, \varepsilon_2)$, accompanied by the baryon number density jump $n_0 = n_{01} \rightarrow n_{02}$, by the following condition resulting from the mechanical and chemical equilibrium of the associated phases:

$$\bar{\varepsilon}_1 + \frac{\gamma_1}{\gamma_1 - 1} = \bar{\varepsilon}_2 + \frac{\gamma_2}{\gamma_2 - 1} \frac{1}{\lambda}, \quad (5)$$

where

$$\bar{\varepsilon}_i = \frac{\varepsilon_i n_0}{P_0} \quad \text{and} \quad \lambda = \frac{n_{02}}{n_{01}} = \frac{n_{02}}{n_0}. \quad (6)$$

For the mixed state we assume a polytropic EOS given by Eq. (4) with parameters $(K_m, \gamma_m, \varepsilon_m)$. Assuming the appearance of the mixed phase at a pressure $P_1 < P_0$ (and the baryon density $n_1 < n_0$), the parameters γ_m and ε_m of the ‘‘mixed state’’ polytrope are given by the solutions to the following relations:

$$\begin{aligned} \left(\frac{1}{\gamma_2 - 1} - \frac{1}{\gamma_m - 1} \right) \lambda^{\gamma_2(\gamma_m - 1)/(\gamma_2 - \gamma_m)} \times \\ \bar{n}_1^{(\gamma_2 - 1)(\gamma_1 - \gamma_m)/(\gamma_2 - \gamma_m)} + \frac{\gamma_m}{\gamma_m - 1} \bar{n}_1^{\gamma_1 - 1} = \\ \frac{\gamma_2}{(\gamma_2 - 1)} \frac{1}{\lambda} - \frac{\gamma_1}{\gamma_1 - 1} \left(1 - \bar{n}_1^{\gamma_1 - 1} \right), \end{aligned} \quad (7)$$

where $\bar{n}_1 = n_1/n_0 < 1$. The mean ‘‘mixed’’ value of the parameter ε results from

$$\bar{\varepsilon}_m = \bar{\varepsilon}_1 + \left(\frac{\gamma_1}{\gamma_1 - 1} - \frac{\gamma_m}{\gamma_m - 1} \right) \bar{n}_1^{\gamma_1 - 1}, \quad (8)$$

whereas the endpoint of the mixed state (P_3, n_3) is determined by

$$\frac{\bar{P}_3}{\bar{n}_3} = \frac{\bar{n}_3^{\gamma_2 - 1}}{\lambda^{\gamma_2}} = \frac{\bar{\varepsilon}_m - \bar{\varepsilon}_2}{\gamma_2/(\gamma_2 - 1) - \gamma_m/(\gamma_m - 1)}. \quad (9)$$

where $\bar{P}_3 = P_3/P_0$.

Relativistic polytropes are used to define the dense ($n > n_{cc}$, where the subscript cc denote the crust-core transition) part of the EOS. For the low-density part (the crust) we use the Douchin and Haensel SLy4 EOS [54]. The SLy4 crust extends up to the pressure P_{cc} , densities n_{cc} , ρ_{cc} and chemical potential μ_{cc} . At $P = P_{cc}$, we

¹ The $\gamma = 1$ case needs a separate treatment (logarithmic dependence of $\rho(n)/n$) and is not considered here.

define a smooth crust/core transition to the polytrope $P = K_1 n^{\gamma_1}$ with one free parameter γ_1 , and the other two parameters (K_1, m_1) defined by:

$$K_1 = \frac{P_{cc}}{n_{cc}^{\gamma_1}} \quad \text{and} \quad \varepsilon_1 = \mu_{cc} - \frac{\gamma_1}{\gamma_1 - 1}. \quad (10)$$

At (P_0, n_0) , a first-order phase transition between the polytropes $(K_1, \gamma_1, \varepsilon_1)$ and $(K_2, \gamma_2, \varepsilon_2)$ (“Maxwell construction”) is defined by the parameters in Eqs. (5) and (6). A polytrope with selected γ_2 and (K_2, m_2) resulting from the equilibrium conditions is given by

$$K_2 = \frac{P_0}{(\lambda n_0)^{\gamma_2}} \quad \text{and} \quad \bar{\varepsilon}_2 = \bar{\varepsilon}_1 + \frac{\gamma_1}{\gamma_1 - 1} - \frac{\gamma_2}{\gamma_2 - 1} \frac{1}{\lambda}. \quad (11)$$

The mixed state is defined between P_1 and P_3 , associated with the baryon numbers n_1 and n_3 , respectively, with the point $P_1(n_1)$ being a free quantity to choose. With Eqs. (7)-(9) one obtains the parameters of the mixed-phase polytrope and the point (P_3, n_3) . In general, for the mixed state,

$$P_m = P_1 \left(\frac{n}{n_1} \right)^{\gamma_m} \quad \text{and} \quad K_m = P_1 / n_1^{\gamma_m}. \quad (12)$$

Note that the model described in Sect. II A in the mixed region is also a specific case of a polytrope ($\gamma_m = 2$) with an additional pressure term, equal to $(1 + \Delta_p)P_0 - \alpha_1^2/(2\alpha_2)$.

III. TOV EQUATIONS AND TIDAL DEFORMABILITY

The $M - R$ sequences associated with the EOSs of Sec. II come from the solution of the TOV system of equations, namely,

$$\frac{dP}{dr} = -\frac{\rho m}{r^2} \left(1 + \frac{P}{\rho} \right) \left(1 + \frac{4\pi P r^3}{m} \right) \left(1 - \frac{2m}{r} \right)^{-1} \quad (13)$$

$$\frac{dm}{dr} = 4\pi r^2 \rho, \quad (14)$$

where m is the gravitational mass within the radial distance r from the center of the star. The background metric is

$$ds^2 = -e^{\nu(r)} dt^2 + e^{\lambda(r)} dr^2 + r^2(d\theta^2 + \sin^2\theta d\phi^2), \quad (15)$$

with ν given by

$$\frac{d\nu}{dr} = -\frac{2}{\rho + P} \frac{dP}{dr}. \quad (16)$$

The metric function λ is related with m by means of

$$e^{\lambda(r)} = \left[1 - \frac{2m(r)}{r} \right]^{-1}. \quad (17)$$

For each background configuration, we have also calculated its tidal deformability. We have assumed perfect-fluids all along. Although some phases of NSs—especially the mixed states—should be elastic, we do not take into account this fact in this first study. The equation that we solve related to tidal deformations is [55, 56]

$$H_0'' + \mathcal{A}_1 H_0' + \mathcal{A}_0 H_0 = 0, \quad (18)$$

where

$$\begin{aligned} \mathcal{A}_0 \equiv & \nu'' - \frac{6e^\lambda}{r^2} - \frac{(\nu')^2}{2} + \frac{3\lambda' + 7\nu'}{2r} \\ & - \frac{\nu'\lambda'}{2} + \frac{\rho'}{P'} \frac{\nu' + \lambda'}{2r} \end{aligned} \quad (19)$$

and

$$\mathcal{A}_1 \equiv \frac{2}{r} + \frac{\nu' - \lambda'}{2}. \quad (20)$$

Tidal deformations themselves (dimensionless) are defined as $\Lambda \equiv 2/3(M/R)^{-5} k_2$, where the Love number k_2 , in terms $y \equiv RH_0'(R)/H_0(R)$, is [55–58]

$$\begin{aligned} k_2 = & 8C^5(1 - 2C)^2[2 + 2C(y - 1) - y] \\ & / (5\{2C[6 - 3y + 3C(5y - 8)] \\ & + 4C^3[13 - 11y + C(3y - 2) + 2C^2(1 + y)] \\ & + 3(1 - 2C)^2[2 - y + 2C(y - 1)] \ln(1 - 2C)\}), \end{aligned} \quad (21)$$

with $C \equiv M/R$ is the compactness of the background star. Therefore, it is clear that one needs to find the interior solution to H_0 and evaluate it on the surface of the star to obtain Λ .

The boundary (interface) conditions that we use here are the continuity of H_0 and H_0' at the borders of the mixed state (with the quark and hadronic phases). This is the case since there is no density jumps when the mixed state is taken into account, due to Eqs. (2) and (3) and the thermodynamic relation $\mu = (P + \rho)/n$. At the center and on the surface of the star, a regular solution and the absence of energy jumps are considered, respectively (for further details, see [59, 60] and references therein). For the tidal deformation calculations in stars with sharp phase transitions, a nontrivial boundary condition at the hadron-quark interface for H_0' should be taken due to the discontinuity of the energy density there (see, e.g., Eq. (41) of [59]).

We stress that Eq. (18) is valid only for perfect fluids in the adiabatic limit. In terms of a binary coalescence, it would be related to the inspiral phase. If parts of the star are elastic, Eq. (18) must be replaced by a set of coupled equations that take into account their shear moduli (see, e.g., [59, 60]). Such equations are much more involved and lead to the intuitive result that tidal deformations of elastic stars are smaller than their perfect-fluid counterparts. In most cases, however, the differences are negligible [59, 60]. Even if the differences are not small, perfect-fluid calculations would lead to larger

values, and hence the maximum changes between configurations with sharp and mixed states. Therefore, even though the mixed state should be elastic, we assume in this work it can be approximated by a perfect-fluid. Any allowed EOS in the perfect-fluid case will also be allowed in the more realistic case with elasticity.

IV. RESULTS

Exemplary sequences of sharp- and mixed-state EOSs, based on the polytropic approach of Sect. II B, are presented in Fig. 1. The parameters of the EOSs are given in its caption. In the following, we will first discuss the origin of the similarity of the M_{\max} and $R_{M_{\max}}$ for both types of state transitions, and then estimate the sizes of the differences using the EOS approximations from Sect. II B and II A.

A. Equality of M_{\max} and other global stellar parameters

The radial dependence of the baryon chemical potential (Gibbs energy per baryon) is obtained from:

$$\frac{d \ln \mu}{dr} = \frac{m}{r^2} \frac{(1 + 4\pi r^3 P/m)}{1 - 2m/r}, \quad (22)$$

while the quantity m can be calculated using:

$$\frac{dP}{dm} = \frac{m}{4\pi r^4} \frac{(1 + 4\pi r^3 P/m)(1 + P/\rho)}{1 - 2m/r}. \quad (23)$$

For the central pressure larger than the pressure P_3 , at which a mixed state is fully present in the interior of the star, its region is represented by a shell of thickness $\Delta r_{\text{mixed}} = r(P_1) - r(P_3)$ and a mass $\Delta m_{\text{mixed}} = m(P_1) - m(P_3)$. Global parameters of this mixed shell, as well as a shell containing the sharp phase transition between (μ_1, P_1) and (μ_3, P_3) are calculated from Eqs. (22) and (23), and weakly depend on the kind of the EOS (i.e., sharp or mixed) in this region. Equation (13) from [61] can be used to estimate the thickness of the mixed state region, however it should be stressed that the parameters neglected for the crust ($r^3 P/m$, the change of mass in the considered region) are more important in our case ($P/\rho \simeq 0.1$). As a result, the mass-radius relations for the first order phase transition and the mixed state are almost identical in the regions above (P_3, μ_3) . This is exemplified in the next section with the use of many polytropic EOSs.

B. Results for polytropic EOSs

In order to decide which cases might be observationally relevant, we make use of already existing and future mass, radius and tidal deformation measurement

accuracies. NICER measurements already allow the constraint of masses and radii of NSs with relative uncertainties around 5% (for combined observations), and around 10% for single observations (see, e.g., [11] and references therein) at 1σ level. Future missions, such as eXTP or Athena are expected to measure the above quantities with even smaller fractional uncertainties, around a few percent (say, 1–2% in the most optimistic cases; at the 90% credible interval, uncertainties would increase accordingly). When it comes to tidal deformations, current relative uncertainties are still large ($\sim 50 - 100\%$), but future measurements (e.g., with third generation GW detectors) could deliver uncertainties as small as 2% at the 90% credible level in the most optimistic cases [62]. For 2.5-generation detectors and less optimistic cases, relative uncertainties of 5–10% are expected [62]. When translated to radius constraints, they could also be around a few percent (1–2%) for the most optimistic cases at the same credible level as above [62].

The effectiveness of the approximation from Sect. IV A is demonstrated by comparing a large set of sharp phase transition EOSs with their corresponding mixed-state EOSs. The prescription is based on the polytropic approximation of Sect. II B, where the values of polytropic indices and baryon densities, denoting the beginnings and ends of the phases, cover the following ranges: $\gamma_1 \in (2.75, 3.75)$, $\gamma_2 \in (4.5, 6.5)$, $n_0 \in (0.4, 0.5) \text{ fm}^{-3}$, $n_{02}/n_0 \in (1.45, 1.65)$ [we only consider here strong phase transitions (large quark-hadron density jumps) in order to maximize observable differences], $n_1 \in (0.325, 0.4) \text{ fm}^{-3}$; γ_m and n_3 were solutions to the thermodynamic conditions and roughly varied in the intervals $(0.5, 2.5)$ and $(0.5, 1.0) \text{ fm}^{-3}$, respectively. These parameter intervals lead to observationally reasonable NS masses, radii and tidal deformations, and also reflect expectations regarding the densities phase transitions might take place in stars (see [32] for further details). For final comparisons, we select only those microscopic models that lead to $M_{\max} > 2 M_{\odot}$, $\mu_m(n_3)/\mu_m(n_{02}) < 1.15$, $\mu_m(n_1)/\mu(n_0) > 0.85$ (see [30] for the reasonableness of these limits). We keep all γ_m fulfilling the above conditions in order to better explore the region of parameters of the mixed state and also to check consistency, given that low mixed phase adiabatic indices would be a rough proxy for sharp phase transition EOSs. Figures 2, 3 and 4 show the differences (sharp phase transitions and mixed states) for the maximum mass, and Fig. 5 shows the radius differences at the maximum mass, as a function of several parameters: Δ_p , $P_m(n_3) - P_m(n_1)$ and $\mu_m(n_3) - \mu_m(n_1)$. One can clearly see that the fractional differences are very small: around $10^{-1}\%$ for the maximum mass and $10^{-3}\%$ for the associated radius. The larger scatter in Fig. 5 is simply due to the general flattening of the mass-radius relation around the maximum mass. In general, smaller values of γ_m lead to smaller differences, as consistency would demand.

Regarding Δr_{mixed} and Δm_{mixed} , Figs. 6 and 7 show how aspects of a mixed state compare with aspects of a

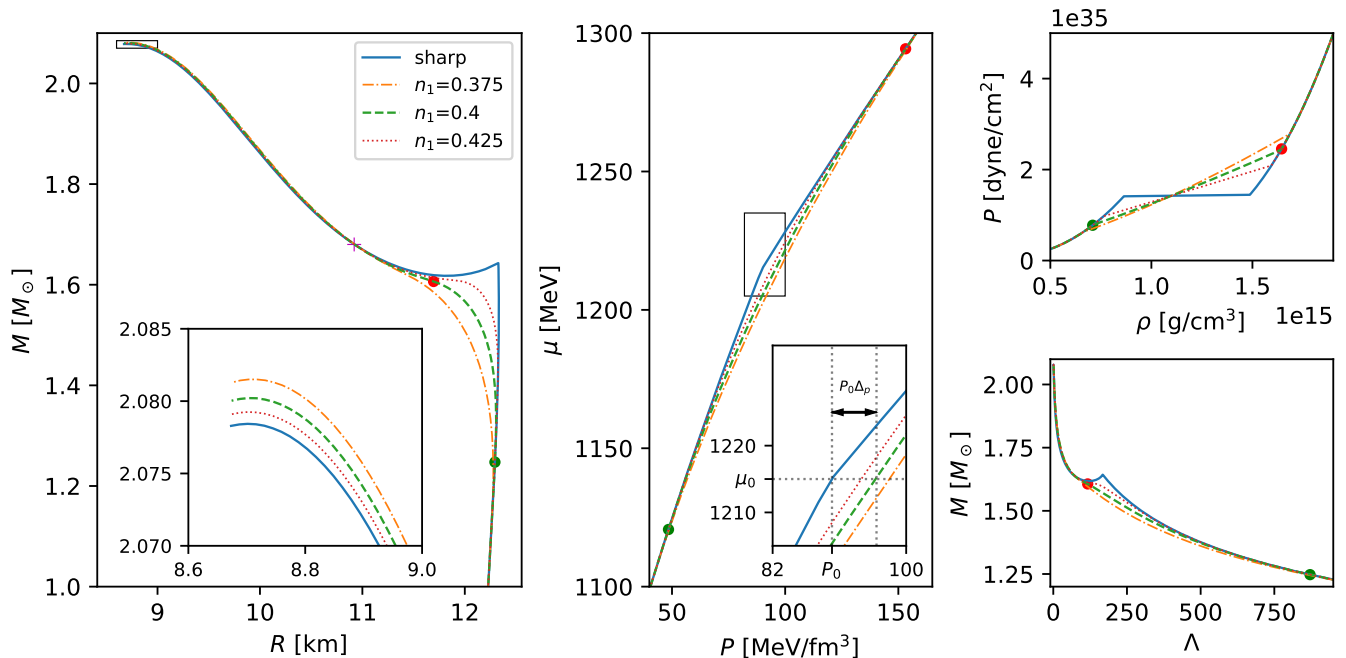


FIG. 1. Examples of polytropic EOSs and resulting sequences of NS parameters (solutions of TOV equations): sharp phase transition (solid blue curves), and three mixed state realizations (dash-dotted orange curves with $n_1=0.375 \text{ fm}^{-3}$, dashed green curves with $n_1=0.4 \text{ fm}^{-3}$ and dotted red curves with $n_1=0.425 \text{ fm}^{-3}$). The sharp phase transition EOS parameters are $\gamma_1 = 3.5$, $\gamma_2 = 6$, density jump (in terms of the baryon density n) between $n_0 = 0.475 \text{ fm}^{-3}$ and $n_02 = 0.76 \text{ fm}^{-3}$, mixed state starting at $n_1 = 0.4 \text{ fm}^{-3}$. The leftmost panel contains the mass-radius $M(R)$ sequences (the inset plot presents a closeup of the region around the maximum mass), the middle panel is the chemical potential-pressure $\mu(P)$ relation, the upper right panel is the pressure-density $P(\rho)$ relation, whereas the lower right one is the mass-tidal deformability $M(\Lambda)$ relation. Green and red dots mark the beginning and the end of the mixed-state region in the case of the $n_1=0.4 \text{ fm}^{-3}$ EOS; correspondingly, stellar configurations in the other panels have central EOS parameters equal to the beginning (green dot) and the end (red dot) of the mixed state. The inset in the $\mu(P)$ plot shows the definition of Δ_p - marked by an arrow - on the example of the $n_1=0.4 \text{ fm}^{-3}$ EOS, marked by the green dashed line. $P(\mu_0)$ is denoted by P_0 . Note that the for the $M(R)$ sequences the mixed state curves are below the sharp one in the vicinity of the phase transition point, but M_{max} is larger for the mixed state EOSs. For the $n_1=0.4 \text{ fm}^{-3}$ EOS, the mixed state and the sharp transition EOSs have the same mass and radius parameters at $M \approx 1.68 M_\odot$ and $\approx 10.92 \text{ km}$, marked by a magenta cross.

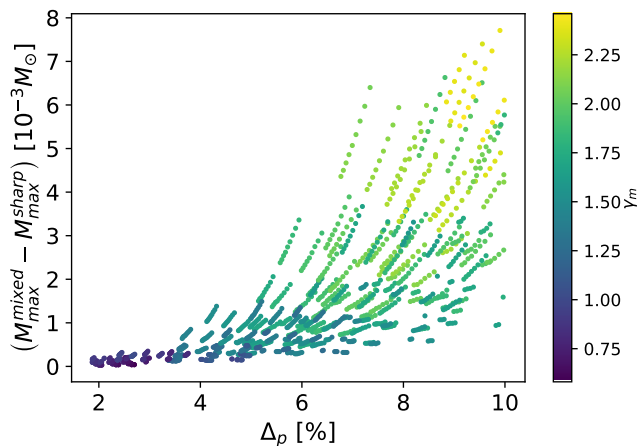


FIG. 2. Mass differences of hybrid stars with mixed states and sharp phase transitions for the maximum masses for several polytropic equations of state as a function of Δ_p .

sharp phase transition for a region between P_1 and P_3 in the case of hybrid stars with the same mass (usually different central pressures). Naturally, in order to do so, we have only taken stars whose P_3 are smaller than their central pressures for given reference masses. One can see that for almost all cases, fractional changes of the mass and the thickness for sharp phase transitions and mixed states are at most of a few percent, and the difference decreases, for a given $P_m(n_3) - P_m(n_1)$, when the mass of the star increases. (That would qualitatively explain why the differences are so small for the maximum masses and associated radii of stars.) The color maps also make it clear that differences between mixed-state and sharp EOS aspects increase with γ_m . This is reasonable given that a mixed-state EOS becomes harder for larger γ_m . When it comes to the fractional radius differences for a given mass, Fig. 8 for $1.4 M_\odot$ (stable) stars suggests that in some cases the differences could be observed by near-term detectors. The largest differences concern purely hadronic (one-phase) stars (whose phase-

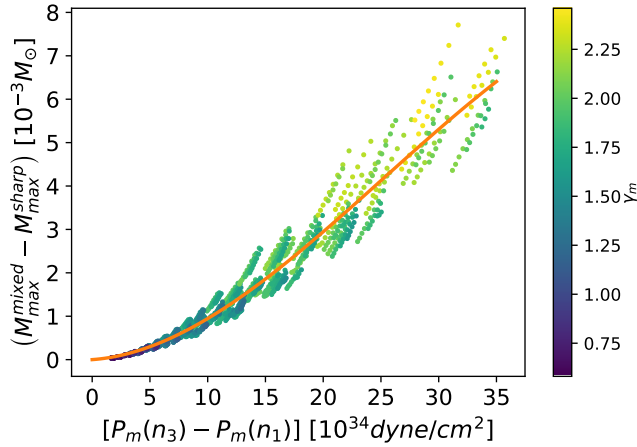


FIG. 3. Same as Fig. 2 but now taking into account the pressure difference between the bottom and the top of the mixed state. The polynomial fit is of the form $y = a_1x + a_2x^2 + a_3x^3$, with $a_1 = 1.8957 \times 10^{-2}$, $a_2 = 8.7218 \times 10^{-3}$ and $a_3 = -1.1525 \times 10^{-4}$.

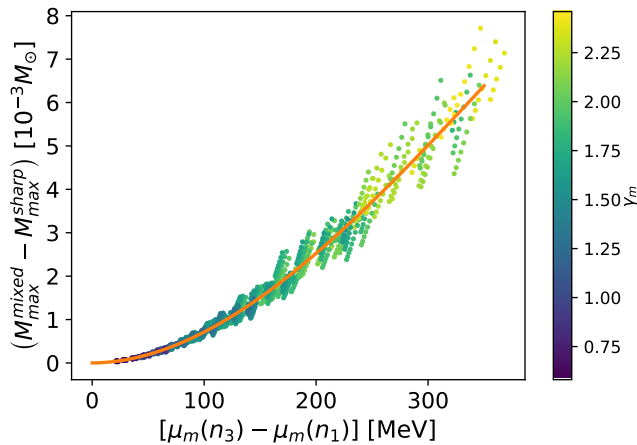


FIG. 4. Maximum mass dependence on the chemical potentials at the borders of the mixed state. Fit: the same of Fig. 2, with $a_1 = 2.4293 \times 10^{-4}$, $a_2 = 7.5863 \times 10^{-5}$ and $a_3 = -6.9803 \times 10^{-8}$.

transition masses are larger than $1.4 M_\odot$) being compared with stars presenting mixed states. If, instead, one restricts the comparison to $1.4 M_\odot$ stars all having quark cores, the radius changes decrease significantly, and are up to around 1-2%. All the above shows that mixed states and sharp phase transitions between P_1 and P_3 almost share the same macroscopic properties, despite being very different physically and encompassing non-negligible portions and masses to stars in general. Indeed, the impact of a mixed state inside a neutron star could be significant, as shown in Fig. 9.

Differences of the thickness of regions between P_1 and P_3 for a sharp-phase-transition and a mixed-state star are up to order 0.5 – 1% when, instead of a same mass, one considers a same central pressure. In this case, maximum

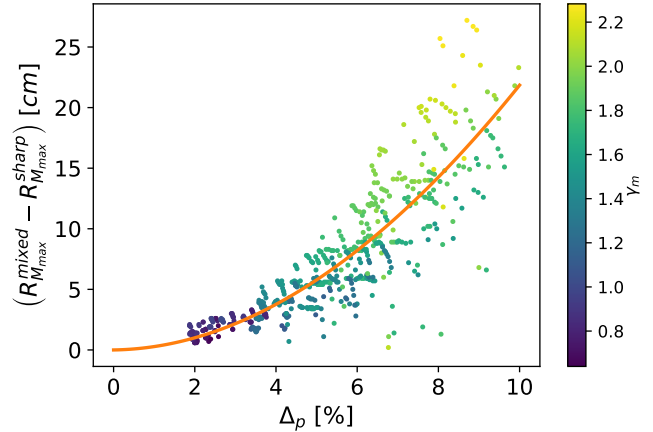


FIG. 5. Radius differences associated with the maximum masses for stars with mixed states and sharp phase transitions for several polytropic equations of state as a function of Δ_p . Third order polynomial fit (same form of Fig. 2): $a_1 = 5.0251 \times 10^{-2}$, $a_2 = 2.2881 \times 10^{-1}$ and $a_3 = -1.5317 \times 10^{-3}$.

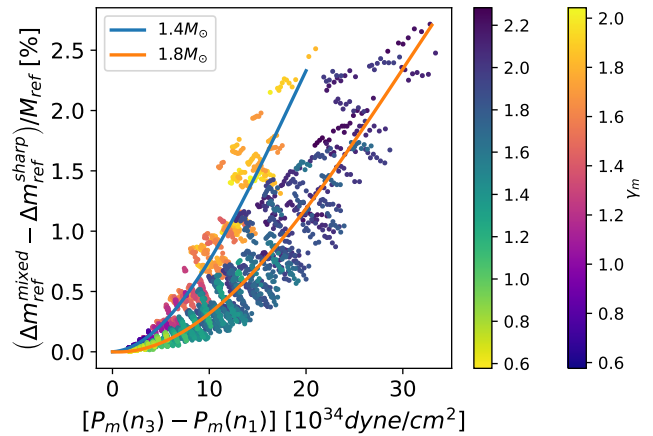


FIG. 6. Mixed state’s masses (within pressures P_1 and P_3) subtracted by masses encompassed within the same pressures in stars with sharp phase transitions, normalized by the reference (“ref”) masses (either 1.4 or 1.8 solar masses). For $1.4 M_\odot$ stars, the third order polynomial fit parameters are $a_1 = 5.1791 \times 10^{-3}$, $a_2 = 8.5127 \times 10^{-3}$ and $a_3 = -1.4737 \times 10^{-4}$. For $1.8 M_\odot$, it follows that $a_1 = -4.6677 \times 10^{-4}$, $a_2 = 4.0884 \times 10^{-3}$ and $a_3 = -4.4263 \times 10^{-5}$.

changes to the mass within the same above pressures would be up to a few percent, given that with the same central pressure the stars would have different masses in general (for the same mass, the central pressure of a star with a mixed state is smaller by a few percent when compared to a star with a sharp phase transition and this dominates the difference in the thickness of the $(P_1 - P_3)$ layers, which are $\sim 5 - 10\%$, about ten times larger than those with the same central pressure).

The presence of a mixed state leads to slightly larger masses between P_1 and P_3 when compared to their sharp-transition counterparts in general because the change of a

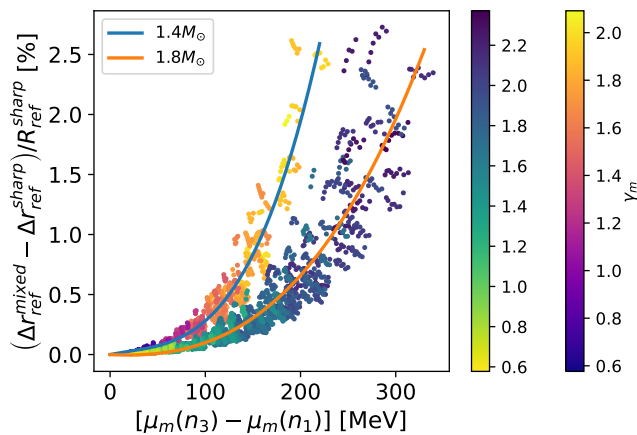


FIG. 7. Thickness differences of the mixed states of stars with respect to sharp phase transitions for the same pressures at the beginning and end of the mixed states, normalized by the radius of stars with sharp phase transitions for the reference masses ($R_{\text{ref}}^{\text{sharp}}$). For $1.4 M_{\odot}$ stars, the fit parameters are $a_1 = 1.5216 \times 10^{-3}$, $a_2 = -1.5230 \times 10^{-5}$ and $a_3 = 2.8132 \times 10^{-7}$. For $1.8 M_{\odot}$, it follows that $a_1 = -3.9125 \times 10^{-4}$, $a_2 = 9.1390 \times 10^{-6}$ and $a_3 = 4.6576 \times 10^{-8}$.

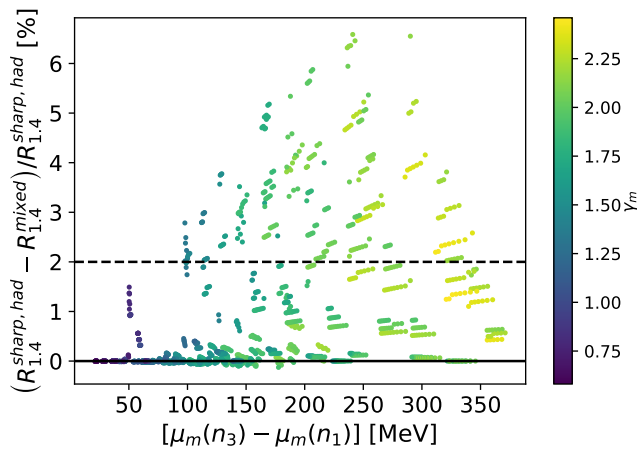


FIG. 8. Relative radius differences for $1.4 M_{\odot}$ stars with mixed states, sharp phase transitions and even purely hadronic (“had”)/one-phase. Here, 2% is a representative level of accuracy of near-future electromagnetic/GW missions. The largest differences are connected with the comparison of one-phase stars with those with mixed states. The smallest differences ($\lesssim (1-2)\%$), though, come from stars with mixed states and those with sharp phase transitions and quark cores.

sharp phase transition’s EOS to a mixed state’s increases the pressure at higher densities, which usually compensates its decrease at lower densities.

When tidal deformations are concerned, fractional changes could be much larger and could exceed the rough threshold of detectability for 3G GW detectors (uncertainties as small as 2%) for certain cases, as clear from Fig. 10 for $1.8 M_{\odot}$ hybrid stars (naively speaking, they

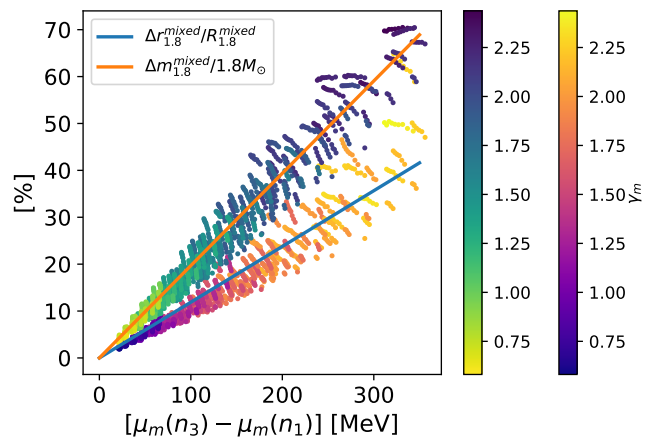


FIG. 9. Relative thicknesses and masses of mixed states in hybrid stars with $1.8 M_{\odot}$. Straight lines ($y = a_1 x$) fit the data; for the relative thickness size of the mixed state, $a_1 = 0.1189$; for its relative mass, $a_1 = 0.1969$. The size and mass of the mixed state is non-negligible when compared to the corresponding aspects of the star in general, and it increases with the increase of γ_m .

are more likely to have quark cores due to larger central pressures than $1.4 M_{\odot}$ stars and also are more likely to be detected than $2 M_{\odot}$ stars in terms of tidal deformations), and Fig. 11 for $1.4 M_{\odot}$ encompassing either hybrid or even one-phase stars. In the case a larger range of stars—even purely hadronic—are compared with those having the same mass but mixed states in their interiors, relative tidal deformations as high as around 40–50% could emerge. Thus, from all the above, tidal deformations may be a relevant observable for distinguishing sharp phase transitions from mixed states in NSs. We come back to this issue later on. The above figures also reveal that depending on where in mass the quark phase appears, the sharp phase transitions could lead to either larger or smaller tidal deformations than mixed states. Therefore, for a given mixed-state EOS, there should exist a critical mass (a “crossing mass”) above which tidal deformations of stars with mixed states are larger than their sharp-phase-transition counterparts, and do not always chase the latter down from below. Figures 1 and 8 also show some aspects of this crossing, which happens at different masses in the $M-R$ and $M-\Lambda$ diagrams, for a particular EOS.

In our set of polytropic EOSs, accidentally, we have not reached very small values for Δ_p (or any other parameter difference between the top and the bottom of the mixed state), due to the particular combination of parameters required for that. However, it is more controllable to do so using the parabolic construction of Abgaryan *et al.* As the plots in the next section will show, when the mixed state is very thin ($\Delta_p \rightarrow 0^+$), the observables converge to the sharp-phase transition ones. That is very clear from the EOS point of view (because they are basically the same), which is the basis for any observable.

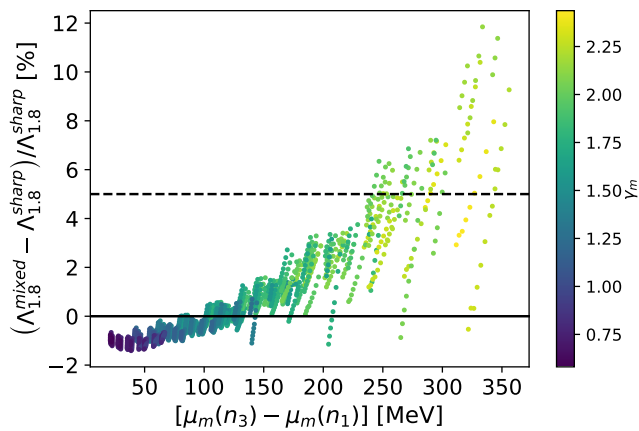


FIG. 10. Relative tidal deformations of $1.8M_{\odot}$ hybrid stars (with mixed states and sharp phase transitions and quark cores) as a function of the chemical potential difference at the beginning and the end of the mixed state. The threshold of around 5% precision is reached for chemical potential differences larger than approximately 250 MeV and $\gamma_m \gtrsim 1.5$.

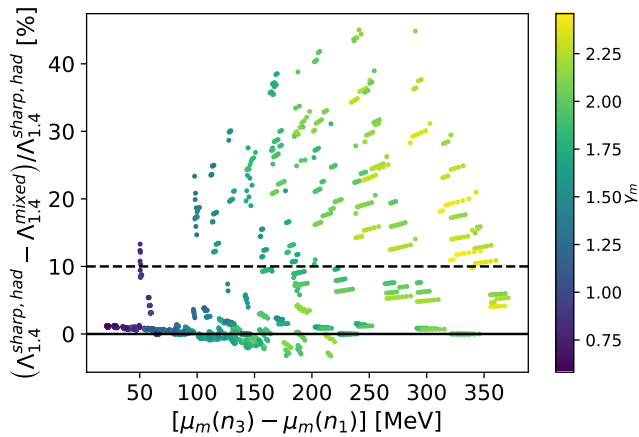


FIG. 11. Relative tidal deformations of $1.4M_{\odot}$ stars relaxing the constraint that they only have quark cores and central pressures larger than the ones fully encompassing the mixed state: here they can also be purely hadronic (“had”) or have mixed states at their centers. The tidal deformation normalization has been chosen to be those of $1.4 M_{\odot}$ stars either presenting sharp phase transitions or being purely hadronic, which depends on the phase transition masses due to their EOSs. The largest differences are obtained when one compares an one-phase star with another one having a mixed state (for a same mass), for large values of γ_m . Fractional differences even exceeding 10% could happen for several EOSs and γ_m s.

C. Results for the Abgaryan *et al.* 2018 construction

The analysis of the large set of polytropic mixed-state EOSs from the previous section has given us many clues on the relevant cases to focus on in terms of observations.

Here we particularize the analysis to the (parabolic) mixed state construction due to Abgaryan *et al.* to draw some additional back-of-the-envelope conclusions regarding observability and to show that different constructions roughly agree among themselves. In addition to the sharp-phase transition EOSs of Sec. II B, we also use here some EOS models explained in detail in [38]. In summary, a simple MIT bag model for the quark core (with $c_s^2 = 1$ to maximize differences) is joined to a polytropic EOS for the inner crust and then, around and below (smaller densities) the nuclear saturation density, the SLy4 EOS is taken into account. The density jump between the quark phase and the polytropic EOS is a free, controllable, parameter.

We have considered some exemplary EOSs with different Δ_p and density jumps, $\eta \equiv \rho_-/\rho_+ - 1$, in order to assess which cases would be more observationally relevant. Here we have defined ρ_- (ρ_+) as the density at the top(base) of the quark(hadronic) phase in the case of the Maxwell construction. Our study is not exhaustive but just representative of the two main cases for phase transitions: weak and strong (see, e.g., [32] and references therein). Weak phase transitions do not violate the Seidov condition for a stable quark phase, $\eta < 1/2(1 + P_0/\rho_+)$ [63], whereas strong ones do. Maxwell constructions fulfilling such a condition could present small quark cores. However, if it is violated, stable quark cores could only be sizable [64].

In particular, due to the existence of the so-called third family of compact stars, strong phase transitions could lead to more pronounced differences when compared to one-phase stars. Therefore, one would expect that the largest differences for the Maxwell and the mixed state predictions would also come from strong phase transitions. We show numerically this is precisely the case. The underlying reason is that strong phase transitions would allow the construction of the mixed state with larger Δ_p .

In our forthcoming analysis we will focus on the benchmark uncertainties relevant for near-term electromagnetic missions and 2.5- and 3rd-generation GW detectors. For the reference values, we mostly take the ones close to the appearance of the quark phase in the Maxwell construction since they maximize the departures from a mixed state and a sharp phase transition.

In Fig. 12 we show a portion of the $M - R$ relation for stars with $\eta = 0.71$ and Δ_p from around 7% (largest possible value as suggested from the surface tension analysis) to 1%, for masses and radii around the sharp phase transition. The EOS related to the Maxwell construction is the same of Fig. 1 for $n_1 = 0.4 \text{ fm}^{-3}$. The value $\Delta_p = 6.7\%$ has been chosen because it coincides with the particularities of the polytropic EOS chosen in the aforementioned figure. Figure 13 shows their associated tidal deformations as a function of the stars’ masses. The boxes on the plots show the range of possibilities for the observables when the mass, radius and tidal deformations have different (small) relative uncertainties according to expectations of near-term and future detectors.

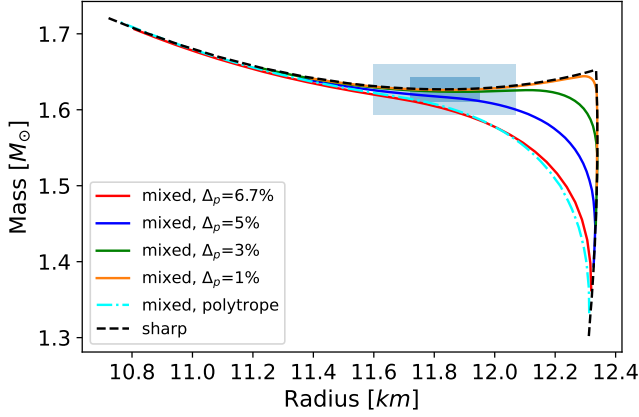


FIG. 12. Mass-radius relations around the appearance of a quark phase for stars with and without the mixed state for $\eta = 0.71$ (same sharp-phase-transition EOS of Fig. 1). The dot-dashed cyan curve is a zoom-in of the correspondent curve in Fig. 1 for a polytropic construction of the mixed state ($n_1 = 0.4 \text{ fm}^{-3}$ EOS) around the appearance of the quark phase. The darker (lighter) box corresponds to masses and radii with (representative) 1% (2%) fractional uncertainties, centered around the critical point for the Maxwell construction ($M = 1.63M_\odot$, $R = 11.84 \text{ km}$).

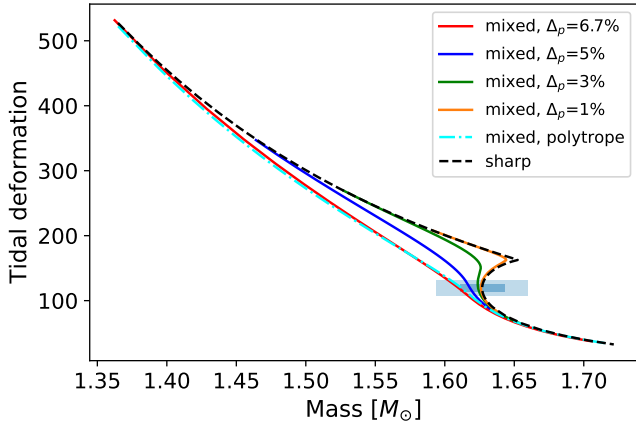


FIG. 13. Mass-tidal deformation relations around the appearance of a quark phase for stars with and without the mixed state for $\eta = 0.71$. The dot-dashed cyan curve is also a zoom-in of the correspondent plot in Fig. 1 for the $n_1 = 0.4 \text{ fm}^{-3}$ EOS. The darker (lighter) box corresponds to tidal deformations with (representative) 5% (10%) fractional uncertainties. The mass uncertainties are the same of Fig.12.

Figures 14 and 15 show similar relations for $\eta = 0.39$. It constitutes a weak phase transition, and the maximum Δ_p for which the parabolic construction works is $\sim 5.3\%$.

From the above-mentioned plots, it is clear that a strong phase transition is the most promising case under the observational point of view. However, present missions may not be able to differentiate between sharp phase transitions and mixed states even for this case. In general, only missions with mass and radius uncertain-

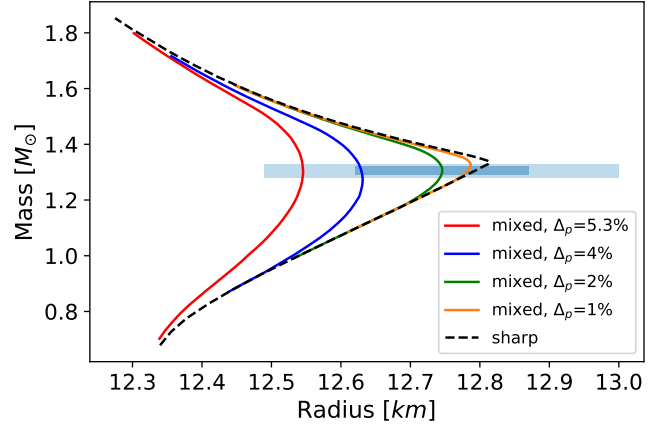


FIG. 14. Same as Fig. 12 but for $\eta = 0.391$. We centered uncertainty boxes at $M = 1.31M_\odot$, $R = 12.75 \text{ km}$ (inflection point of the $\Delta_p = 2\%$ curve).

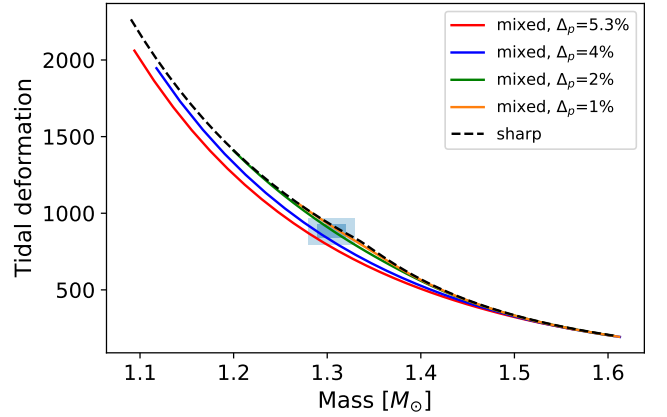


FIG. 15. Same as Fig. 13. The uncertainty boxes are centered at the same mass of Fig.14 and its associated tidal deformation.

ties around 1 – 2% and tidal deformations around 5% or smaller may do it.

Notwithstanding, there may be some exceptions when it comes to tidal deformations, as shown in Fig. 13. In the neighborhood of a strong phase transition, one has a mass range of stable stars with sharp phase transitions whose tidal deformations could differ up to around 25% with respect to stars presenting mixed states. However, differently from strong phase transitions, twin stars may not even exist if Δ_p is large enough. If this is not the case, then, depending on Δ_p , twin stars (one of them being one-phased and the other one with a mixed state) might have any tidal deformation differences (they could be either zero–continuous–or not, as in the cases of $\Delta_p = 3\%$ and $\Delta_p = 1\%$, respectively, in Fig. 13) around the mass marking the appearance of the quark phase (differently from the case of a given strong phase transition), and it could be as large as 50 – 60%, in rough agreement with our analysis for polytropic EOSs in Sec. IV B. If Δ_p is

very small, then it seems unlikely to differentiate mixed states from sharp phase transitions by means of twin stars because their tidal deformations would be very similar. Finally, similarly to Figs. 2, 3 and 4, fractional changes to the maximum mass for different η within the context of the parabolic construction for the mixed state are also up to $\mathcal{O}(0.1\%)$. Radius differences associated with maximum masses are also of $\mathcal{O}(10\text{ cm})$; relative changes of the radii are hence $\mathcal{O}(10^{-3}\%)$. All the above is expected based on the fact that for the maximum masses and associated radii the mixed state outcomes are almost indistinguishable from sharp-phase transition star under the same pressures and hence the particularities of an EOS construction are partially masqueraded.

V. DISCUSSION AND CONCLUSIONS

The existence of a mixed state in an NS is still an open problem in astrophysics. Although expected under the theoretical point of view, there is not yet a direct observation for its presence. This issue is actually nontrivial because it is not any observable that could easily show the imprints of a mixed state. In addition, uncertainties may also thwart attempts to probe its existence. In this work we have tried to identify some observables that may evidence the mixed state. When it comes to radius observations in general, it seems that only future missions with relative radius and mass uncertainties smaller than 1 – 2%, may be relevant. Tidal deformations should also be well constrained in general (fractional uncertainties smaller than 5 – 10%). However, for a range of masses close to the appearance of the quark phase in the case of strong phase transitions, tidal deformations associated with sharp interfaces and mixed states may differ more significantly. For instance, as suggested by Fig. 13, the relative change between a hybrid star with a stable quark core and another one with mixed state and the same mass could be up to around 25%. Twin stars may not even exist if the mixed state has a large enough Δ_p . That is also the case for purely nucleonic stars, and interpretative ambiguities might still persist. If twin stars exist and they are such that one is one-phase and the other one has a mixed state, then relative tidal deformations depend on Δ_p and may take any values, possibly as large as 50% (see Fig. 11). Roughly, the above results agree for different constructions of a mixed state. All of this may give us hope to start probing the existence of the mixed state (or weakly constraining it) in the near future. In particular, the most promising region of the $M - R$ diagram for differentiating a sharp phase transition from a mixed state is around the phase transition mass, and in principle it could happen around and between the most commonly observed masses for NSs ($1.4M_\odot$ and $1.8M_\odot$ [65]).

However, statistical studies also suggest that the phase transition mass may be large, around $2M_\odot$ [66]. If this turns out to be the case, then detectable differences in

tidal deformation measurements for less massive stars would hint that some of them may have mixed states in their interiors. Indeed, the threshold mass characterizing its appearance should be smaller than in the sharp case, and relative tidal deformation changes should be more pronounced. Notwithstanding, a similar conclusion would follow (large differences in tidal deformations and also radii) if one assumed that hadron-quark phase transitions happen at smaller masses (see, e.g., [67] and references therein). A promising way to disentangle sharp phase transitions from mixed states is with a large sample of observations/higher signal-to-noise ratios (SNRs). Many tidal deformation observations for different masses and SNRs could also put radius uncertainties down [62], and this knowledge may differentiate sharp and mixed EOSs. In particular, if mixed states exist, one would expect in general a smoother difference in radius and tidal deformations for different masses than in the case of sharp phase transitions.

Despite the fact that a mixed state can occupy a significant size of a star and contribute non-negligibly to its mass, when it is compared to the same pressure region of a star presenting a sharp phase transition their differences in size and mass are very small, up to a few percent. As a result, this leads a sharp phase transition and a mixed state EOS to present very similar $M - R$ relations away from the phase transition mass region. This is similar to the masquerade problem in (weak) sharp phase transitions when compared to purely hadronic stars. A qualitative explanation for this is that the mixed state EOS is constructed in a way that the increase of pressure in denser regions is followed by the decrease of pressure in lower densities, leading, roughly, to a zero-sum game, as is the case in sharp phase transitions. We have found that the mass and radius differences decrease with the increase of the mass, which would make it more difficult to differentiate sharp phase transitions and mixed states with masses and radii measurements alone if phase transitions happen at large masses.

Characterizing a mixed state seems a much more complicated task than probing its existence. There are different ways of constructing it, although they lead to similar descriptions. We have focused on phenomenological descriptions building on the Maxwell construction. This makes sense because a sharp phase transition is the limit of a very thin layer in a mixed state (as our analysis pertaining to the parabolic and polytropic constructions clearly show). One of the reasons for different constructions leading to similar aspects is their sharing of key thermodynamic conditions, and also the fact that the mixed state's structure is only relevant for a limited range of chemical potentials. Importantly, in the range of masses where a sharp transition would differ the most from another one with a mixed state, different constructions for the mixed state are expected to lead to very small systematic uncertainties. In the example of Figs. 12 and 13, relative changes for the tidal deformations intrinsically associated with different models are up to

approximately 1%. Fractional changes to the radius due to the mixed state modelling are much smaller, up to around 0.2%. This would suggest that third generation GW detectors and future electromagnetic missions may characterize some aspects to the mixed state in a rather model independent way.

The surface tension is one of the key ingredients connecting strong interactions of the matter constituents and the phenomenology of a mixed state in a hybrid star. First of all, the very existence of the structured mixed state layer is due to a nonvanishing surface tension σ at an exotic-normal matter interface. For $\sigma = 0$, the exotic and normal phases are perfectly mixed with no finite-size substructures, while for $\sigma \geq \sigma_{\max}$ no mixed state is allowed, and the Maxwell construction of the exotic phase coexisting with the normal phase at a well-defined pressure holds. The appearance of substructures with different shapes is related to the interplay between Coulomb and surface energies (the Coulomb energy being related to the surface one via the virial theorem [33]). For $0 < \sigma < \sigma_{\max}$, positive surface plus Coulomb contribution (the so-called finite-size effects) to the macroscopic energy density are more than balanced out by the decrease of the bulk energies of the normal and exotic components. The thickness of the mixed state layer is anticorrelated with the surface tension. The transition from the normal phase to the mixed state with an increasing pressure keeps the energy density and the baryon density continuous, and only the sound speed drops discontinuously. Then, the transition from the mixed state to the exotic one, while keeping densities continuous, is associated with a jump in the speed of sound.

Coexisting substructures of exotic and normal phases, e.g., droplets, columns, plates and corresponding bubbly structures, are electrically charged. To minimize the energy in the mixed state, the equilibrium mixed state has a periodic crystal ordering [34]. The mixed state resists deformation via an elastic strain, which contributes to the matter stress tensor. In this way, the hydrostatic equilibrium of an NS becomes the hydro-elastic one (e.g., [38]). A rough estimate of the maximum ellipticity of a solitary hybrid NS, supported by elastic strain of its mixed hybrid core, was obtained by [68]. It will be of interest to address this aspect of the mixed state and in particular its imprint on Λ , and we will do so in a follow up paper.

Our analysis suggests that differentiating a weak (sharp) phase transition from a mixed state will be much more observationally challenging. A reason for so is the intrinsically smoother (and smaller) change of observables in this phase transition case when compared to a strong one. As a result, the lack of observable differences between sharp and mixed EOS aspects might put upper limits on the density change from a hadronic to a quark phase (current multimessenger constraints are yet loose [69–71]) and Δ_p . These upper-limits could also be translated into limits to σ given microscopic models. This would be relevant due to our current ignorance on this quantity. One may also roughly estimate the required

SNR to differentiate between a weak phase transition and a mixed state. Figure 15 suggests that relative tidal deformation uncertainties should be of the order of a few percent, say 1–2%. Given that large SNRs scale inversely with uncertainties [72], for a GW170817-like event one would need an SNR $\approx 2000 - 3500$ to distinguish a phase transition with a mixed state from a weak (sharp) one. This is larger than the most optimist expectations for the Einstein Telescope (see, e.g., [62, 72] and references therein).

Other quantities worth exploring in order to single out aspects of the mixed state would be the moment of inertia of stars and their quadrupole moments. They would be relevant due to the prospect of near future measurements of the rate of advance of the periastron and ellipticities of stars, respectively. Indeed, it will be possible to measure the rate of the advance for some sources [73], and now we are closer to measuring mountains in NSs with GWs (see, e.g., [74–77] and references therein). In the vein of GWs, an elastic mixed state might be able to heighten mountains in the crust, and details thereof should be better understood. For third generation detectors, it would also be of interest to calculate the quasi-normal modes of a hybrid star with a mixed state because some modes might rise uniquely due to it in the range of hundreds to some kHz. In this case, the planned GW mission NEMO [48] might also be relevant. It is a 2.5-generation GW detector that will sacrifice sensitivity at low frequencies to obtain larger-than-current sensitivities in the high frequency band. As a result, it will be suitable for GW observations of the late inspiral and the post-merger phases of binary coalescences. Of particular interest is when one of the compact systems is an NS, because the detection of kHz GWs may unveil unique aspects pertaining to hybrid stars [78, 79]. In addition, when combined to Advanced LIGO and many detections are available, it may also be able to better constrain NS EOSs due to tidal deformation measurements (larger impact on the waveforms). The expected (fractional) radius precision is not far off from the one we have estimated to start evidencing the presence of a mixed state layer. Thus, mostly when many observations are present, NEMO may also have the potential of shedding light on some aspects of phase transitions in NSs.

VI. SUMMARY

Hybrid stars with sharp phase transitions and mixed states may be distinguished observationally either (i) using data from the GW detectors with tidal deformation uncertainties smaller than 5 – 10%, suggesting that unless we witness rare nearby events with high SNRs, we need to rely in general on 2.5- and 3rd generation GW detectors, or (ii) using electromagnetic missions/GW detectors that could deliver radius and masses uncertainties smaller than 1-2%. The most promising cases concern strong phase transitions (large density jumps for the

Maxwell construction) and stars with mixed states and large Δ_p (the relative pressure change at the chemical potential related to the appearance of the quark phase for a sharp phase transition). Sharp weak phase transitions (smaller density jumps), due to their possibility of having any size for quark cores, seem more challenging to be observationally differentiated from stars presenting mixed states. Upon many observations of similar masses, if no difference is measured for the target observables, limits to some EOS aspects, such as quark-hadron density jump, Δ_p and surface tension, may be obtained. In general, the mixed state would change negligibly the maximum masses of stars and their associated radii when compared to sharp phase transitions. The range of NS masses where changes between sharp phase transition and mixed state observables may be noticeable with near-term and future detectors is around the appearance of a quark phase, and particularities of the mixed state construction are expected to lead to very

small systematic uncertainties. This suggests that constraints to the mixed state might be possible and rather EOS-free.

ACKNOWLEDGMENTS

We thank Nikolaos Stergioulas for useful comments. The Authors gratefully acknowledge the financial support of the National Science Center Poland grants no. 2016/22/E/ST9/00037 and 2018/29/B/ST9/02013, and the Italian Istituto Nazionale di Fisica Nucleare (INFN), the French Centre National de la Recherche Scientifique (CNRS) and the Netherlands Organization for Scientific Research (NWO), for the construction and operation of the Virgo detector and the creation and support of the EGO consortium.

-
- [1] P. Haensel, A. Y. Potekhin, and D. G. Yakovlev, *Neutron Stars 1 : Equation of State and Structure*, Vol. 326 (New York, USA: Springer, 2007) pp. pp.1–619.
- [2] K. Fukushima and T. Hatsuda, The phase diagram of dense QCD, *Reports on Progress in Physics* **74**, 014001 (2011), arXiv:1005.4814 [hep-ph].
- [3] T. Ablyazimov, A. Abuhoza, R. P. Adak, M. Adamczyk, K. Agarwal, M. M. Aggarwal, Z. Ahammed, F. Ahmad, N. Ahmad, and et al., Challenges in QCD matter physics -The scientific programme of the Compressed Baryonic Matter experiment at FAIR, *European Physical Journal A* **53**, 60 (2017), arXiv:1607.01487 [nucl-ex].
- [4] C. Ratti, Lattice QCD and heavy ion collisions: a review of recent progress, *Reports on Progress in Physics* **81**, 084301 (2018), arXiv:1804.07810 [hep-lat].
- [5] M. G. Alford, A. Schmitt, K. Rajagopal, and T. Schäfer, Color superconductivity in dense quark matter, *Reviews of Modern Physics* **80**, 1455 (2008), arXiv:0709.4635 [hep-ph].
- [6] E. S. Fraga, A. Kurkela, and A. Vuorinen, Neutron star structure from QCD, *European Physical Journal A* **52**, 49 (2016), arXiv:1508.05019 [nucl-th].
- [7] G. Baym, T. Hatsuda, T. Kojo, P. D. Powell, Y. Song, and T. Takatsuka, From hadrons to quarks in neutron stars: a review, *Reports on Progress in Physics* **81**, 056902 (2018), arXiv:1707.04966 [astro-ph.HE].
- [8] M. G. Orsaria, G. Malfatti, M. Mariani, I. F. Ranea-Sandoval, F. García, W. M. Spinella, G. A. Contrera, G. Lugones, and F. Weber, Phase transitions in neutron stars and their links to gravitational waves, *Journal of Physics G Nuclear Physics* **46**, 073002 (2019), arXiv:1907.04654 [astro-ph.HE].
- [9] M. C. Miller, F. K. Lamb, A. J. Dittmann, S. Bogdanov, Z. Arzoumanian, K. C. Gendreau, S. Guillot, A. K. Harding, W. C. G. Ho, J. M. Lattimer, R. M. Ludlam, S. Mahmoodifar, S. M. Morsink, P. S. Ray, T. E. Strohmayer, K. S. Wood, T. Enoto, R. Foster, T. Okajima, G. Prigozhin, and Y. Soong, PSR J0030+0451 Mass and Radius from NICER Data and Implications for the Properties of Neutron Star Matter, *ApJ* **887**, L24 (2019), arXiv:1912.05705 [astro-ph.HE].
- [10] T. E. Riley, A. L. Watts, S. Bogdanov, P. S. Ray, R. M. Ludlam, S. Guillot, Z. Arzoumanian, C. L. Baker, A. V. Bilous, D. Chakrabarty, K. C. Gendreau, A. K. Harding, W. C. G. Ho, J. M. Lattimer, S. M. Morsink, and T. E. Strohmayer, A NICER View of PSR J0030+0451: Millisecond Pulsar Parameter Estimation, *ApJ* **887**, L21 (2019), arXiv:1912.05702 [astro-ph.HE].
- [11] M. C. Miller, F. K. Lamb, A. J. Dittmann, S. Bogdanov, Z. Arzoumanian, K. C. Gendreau, S. Guillot, W. C. G. Ho, J. M. Lattimer, M. Loewenstein, S. M. Morsink, P. S. Ray, M. T. Wolff, C. L. Baker, T. Cazeau, S. Manthripragada, C. B. Markwardt, T. Okajima, S. Pollard, I. Cognard, H. T. Cromartie, E. Fonseca, L. Guillemot, M. Kerr, A. Parthasarathy, T. T. Pennucci, S. Ransom, and I. Stairs, The Radius of PSR J0740+6620 from NICER and XMM-Newton Data, *ApJ* **918**, L28 (2021), arXiv:2105.06979 [astro-ph.HE].
- [12] T. E. Riley, A. L. Watts, P. S. Ray, S. Bogdanov, S. Guillot, S. M. Morsink, A. V. Bilous, Z. Arzoumanian, D. Choudhury, J. S. Deneva, K. C. Gendreau, A. K. Harding, W. C. G. Ho, J. M. Lattimer, M. Loewenstein, R. M. Ludlam, C. B. Markwardt, T. Okajima, C. Prescod-Weinstein, R. A. Remillard, M. T. Wolff, E. Fonseca, H. T. Cromartie, M. Kerr, T. T. Pennucci, A. Parthasarathy, S. Ransom, I. Stairs, L. Guillemot, and I. Cognard, A NICER View of the Massive Pulsar PSR J0740+6620 Informed by Radio Timing and XMM-Newton Spectroscopy, *ApJ* **918**, L27 (2021), arXiv:2105.06980 [astro-ph.HE].
- [13] G. Raaijmakers, S. K. Greif, K. Hebeler, T. Hinderer, S. Nisanke, A. Schwenk, T. E. Riley, A. L. Watts, J. M. Lattimer, and W. C. G. Ho, Constraints on the dense matter equation of state and neutron star properties from NICER’s mass-radius estimate of PSR J0740+6620 and multimessenger observations, arXiv e-prints , arXiv:2105.06981 (2021), arXiv:2105.06981 [astro-ph.HE].

- [14] É. É. Flanagan and T. Hinderer, Constraining neutron-star tidal Love numbers with gravitational-wave detectors, *Phys. Rev. D* **77**, 021502 (2008), arXiv:0709.1915 [astro-ph].
- [15] E. D. Van Oeveren and J. L. Friedman, Upper limit set by causality on the tidal deformability of a neutron star, *Phys. Rev. D* **95**, 083014 (2017), arXiv:1701.03797 [gr-qc].
- [16] B. P. Abbott, R. Abbott, T. D. Abbott, F. Acernese, K. Ackley, C. Adams, T. Adams, P. Addesso, R. X. Adhikari, and V. B. Adya, Gravitational Waves and Gamma-Rays from a Binary Neutron Star Merger: GW170817 and GRB 170817A, *ApJ* **848**, L13 (2017), arXiv:1710.05834 [astro-ph.HE].
- [17] B. P. Abbott, R. Abbott, T. D. Abbott, F. Acernese, K. Ackley, C. Adams, T. Adams, P. Addesso, R. X. Adhikari, V. B. Adya, C. Affeldt, M. Afrough, B. Agarwal, M. Agathos, K. Agatsuma, N. Aggarwal, O. D. Aguiar, L. Aiello, A. Ain, P. Ajith, B. Allen, and G. Allen, GW170817: Observation of Gravitational Waves from a Binary Neutron Star Inspiral, *Phys. Rev. Lett.* **119**, 161101 (2017), arXiv:1710.05832 [gr-qc].
- [18] P. Landry, R. Essick, and K. Chatziioannou, Nonparametric constraints on neutron star matter with existing and upcoming gravitational wave and pulsar observations, *Phys. Rev. D* **101**, 123007 (2020), arXiv:2003.04880 [astro-ph.HE].
- [19] R. Essick, P. Landry, and D. E. Holz, Nonparametric inference of neutron star composition, equation of state, and maximum mass with GW170817, *Phys. Rev. D* **101**, 063007 (2020), arXiv:1910.09740 [astro-ph.HE].
- [20] P. T. H. Pang, T. Dietrich, I. Tews, and C. Van Den Broeck, Parameter estimation for strong phase transitions in supranuclear matter using gravitational-wave astronomy, *Physical Review Research* **2**, 033514 (2020), arXiv:2006.14936 [astro-ph.HE].
- [21] K. Chatziioannou, Neutron-star tidal deformability and equation-of-state constraints, *General Relativity and Gravitation* **52**, 109 (2020), arXiv:2006.03168 [gr-qc].
- [22] V. Dexheimer, L. T. T. Soethe, J. Roark, R. O. Gomes, S. O. Kepler, and S. Schramm, Phase Transitions in Neutron Stars, arXiv e-prints, arXiv:1901.03252 (2019), arXiv:1901.03252 [astro-ph.HE].
- [23] K. Chatziioannou and S. Han, Studying strong phase transitions in neutron stars with gravitational waves, *Phys. Rev. D* **101**, 044019 (2020).
- [24] N. K. Glendenning, Phase transitions and crystalline structures in neutron star cores, *Phys. Rep.* **342**, 393 (2001).
- [25] D. Blaschke and N. Chamel, Phases of Dense Matter in Compact Stars, in *Astrophysics and Space Science Library*, Vol. 457, edited by L. Rezzolla, P. Pizzochero, D. I. Jones, N. Rea, and I. Vidaña (Springer, 2018) p. 337.
- [26] D. E. Alvarez-Castillo and D. B. Blaschke, High-mass twin stars with a multipolytrope equation of state, *Phys. Rev. C* **96**, 045809 (2017), arXiv:1703.02681 [nucl-th].
- [27] M. Alford and A. Sedrakian, Compact Stars with Sequential QCD Phase Transitions, *Physical Review Letters* **119**, 161104 (2017), arXiv:1706.01592 [astro-ph.HE].
- [28] A. Ayriyan, N. U. Bastian, D. Blaschke, H. Grigorian, K. Maslov, and D. N. Voskresensky, Robustness of third family solutions for hybrid stars against mixed phase effects, *Phys. Rev. C* **97**, 045802 (2018), arXiv:1711.03926 [nucl-th].
- [29] J.-E. Christian and J. Schaffner-Bielich, Twin Stars and the Stiffness of the Nuclear Equation of State: Ruling Out Strong Phase Transitions below $1.7 n_0$ with the New NICER Radius Measurements, *ApJ* **894**, L8 (2020), arXiv:1912.09809 [astro-ph.HE].
- [30] K. Maslov, N. Yasutake, D. Blaschke, A. Ayriyan, H. Grigorian, T. Maruyama, T. Tatsumi, and D. N. Voskresensky, Hybrid equation of state with pasta phases, and third family of compact stars, *Phys. Rev. C* **100**, 025802 (2019), arXiv:1812.11889 [nucl-th].
- [31] M. Alford, M. Braby, M. Paris, and S. Reddy, Hybrid Stars that Masquerade as Neutron Stars, *ApJ* **629**, 969 (2005), arXiv:nucl-th/0411016 [nucl-th].
- [32] M. Sieniawska, W. Turczański, M. Bejger, and J. L. Zdunik, Tidal deformability and other global parameters of compact stars with strong phase transitions, *A&A* **622**, A174 (2019), arXiv:1807.11581 [astro-ph.HE].
- [33] N. K. Glendenning, A crystalline quark-hadron mixed phase in neutron stars., *Phys. Rep.* **264**, 143 (1996).
- [34] N. K. Glendenning and S. Pei, Crystalline structure of the mixed confined-deconfined phase in neutron stars, *Phys. Rev. C* **52**, 2250 (1995).
- [35] B. T. Reed, F. J. Fattoyev, C. J. Horowitz, and J. Piekarewicz, Implications of PREX-2 on the Equation of State of Neutron-Rich Matter, *Phys. Rev. Lett.* **126**, 172503 (2021), arXiv:2101.03193 [nucl-th].
- [36] S. N. Zhang, M. Feroci, A. Santangelo, Y. W. Dong, H. Feng, F. J. Lu, K. Nandra, and et al., eXTP: Enhanced X-ray Timing and Polarization mission, in *Space Telescopes and Instrumentation 2016: Ultraviolet to Gamma Ray*, Proceedings of the SPIE, Vol. 9905 (2016) p. 99051Q, arXiv:1607.08823 [astro-ph.IM].
- [37] A. L. Watts, W. Yu, J. Poutanen, S. Zhang, Bhattacharyya, and et al., Dense matter with eXTP, *Science China Physics, Mechanics, and Astronomy* **62**, 29503 (2019), arXiv:1812.04021 [astro-ph.HE].
- [38] J. P. Pereira, M. Bejger, L. Tonetto, G. Lugones, P. Haensel, J. L. Zdunik, and M. Sieniawska, Probing Elastic Quark Phases in Hybrid Stars with Radius Measurements, *ApJ* **910**, 145 (2021), arXiv:2011.06361 [astro-ph.HE].
- [39] J. P. Pereira, C. V. Flores, and G. Lugones, Phase Transition Effects on the Dynamical Stability of Hybrid Neutron Stars, *ApJ* **860**, 12 (2018), arXiv:1706.09371 [gr-qc].
- [40] J. L. Zdunik, M. Bejger, P. Haensel, and E. Gourgoulhon, Phase transitions in rotating neutron stars cores: back bending, stability, corequakes, and pulsar timing, *A&A* **450**, 747 (2006), arXiv:astro-ph/0509806 [astro-ph].
- [41] R. C. Tolman, Static Solutions of Einstein's Field Equations for Spheres of Fluid, *Physical Review* **55**, 364 (1939).
- [42] J. R. Oppenheimer and G. M. Volkoff, On Massive Neutron Cores, *Physical Review* **55**, 374 (1939).
- [43] K. C. Gendreau, Z. Arzumanyan, and T. Okajima, The Neutron star Interior Composition Explorer (NICER): an Explorer mission of opportunity for soft x-ray timing spectroscopy, in *Space Telescopes and Instrumentation 2012: Ultraviolet to Gamma Ray*, Vol. 8443, edited by T. Takahashi, S. S. Murray, and J.-W. A. den Herder, International Society for Optics and Photonics (SPIE, 2012) pp. 322 – 329.
- [44] K. Nandra *et al.*, The Hot and Energetic Universe: A White Paper presenting the science theme motivating

- the Athena+ mission, arXiv e-prints , arXiv:1306.2307 (2013), arXiv:1306.2307 [astro-ph.HE].
- [45] J. Aasi *et al.*, Advanced LIGO, Classical and Quantum Gravity **32**, 074001 (2015), arXiv:1411.4547 [gr-qc].
- [46] F. Acernese *et al.*, Advanced Virgo: a second-generation interferometric gravitational wave detector, Classical and Quantum Gravity **32**, 024001 (2015), arXiv:1408.3978 [gr-qc].
- [47] T. Akutsu *et al.*, KAGRA: 2.5 generation interferometric gravitational wave detector, Nature Astronomy **3**, 35 (2019), arXiv:1811.08079 [gr-qc].
- [48] K. Ackley, V. B. Adya, P. Agrawal, P. Altin, G. Ashton, M. Bailes, E. Baltinas, Barbuio, and et al., Neutron Star Extreme Matter Observatory: A kilohertz-band gravitational-wave detector in the global network, PASA **37**, e047 (2020), arXiv:2007.03128 [astro-ph.HE].
- [49] M. Maggiore, C. Van Den Broeck, N. Bartolo, E. Belgacem, D. Bertacca, M. A. Bizouard, M. Branchesi, S. Clesse, S. Foffa, J. García-Bellido, S. Grimm, J. Harms, T. Hinderer, S. Matarrese, C. Palomba, M. Peloso, A. Ricciardone, and M. Sakellariadou, Science case for the Einstein telescope, J. Cosmology Astropart. Phys. **2020**, 050 (2020), arXiv:1912.02622 [astro-ph.CO].
- [50] D. Reitze, R. X. Adhikari, S. Ballmer, B. Barish, L. Barsotti, G. Billingsley, D. A. Brown, Y. Chen, D. Coyne, R. Eisenstein, M. Evans, P. Fritschel, E. D. Hall, A. Lazarini, G. Lovelace, J. Read, B. S. Sathyaprakash, D. Shoemaker, J. Smith, C. Torrie, S. Vitale, R. Weiss, C. Wipf, and M. Zucker, Cosmic Explorer: The U.S. Contribution to Gravitational-Wave Astronomy beyond LIGO, in *Bulletin of the American Astronomical Society*, Vol. 51 (2019) p. 35, arXiv:1907.04833 [astro-ph.IM].
- [51] V. Abgaryan, D. Alvarez-Castillo, A. Ayriyan, D. Blaschke, and H. Grigorian, Two Novel Approaches to the Hadron-Quark Mixed Phase in Compact Stars, Universe **4**, 94 (2018), arXiv:1807.08034 [astro-ph.HE].
- [52] D. Blaschke, A. Ayriyan, D. E. Alvarez-Castillo, and H. Grigorian, Was GW170817 a Canonical Neutron Star Merger? Bayesian Analysis with a Third Family of Compact Stars, Universe **6**, 81 (2020), arXiv:2005.02759 [astro-ph.HE].
- [53] R. F. Tooper, Adiabatic Fluid Spheres in General Relativity., ApJ **142**, 1541 (1965).
- [54] F. Douchin and P. Haensel, A unified equation of state of dense matter and neutron star structure, A&A **380**, 151 (2001), arXiv:astro-ph/0111092 [astro-ph].
- [55] T. Hinderer, Tidal Love Numbers of Neutron Stars, ApJ **677**, 1216 (2008), arXiv:0711.2420.
- [56] T. Hinderer, B. D. Lackey, R. N. Lang, and J. S. Read, Tidal deformability of neutron stars with realistic equations of state and their gravitational wave signatures in binary inspiral, Phys. Rev. D **81**, 123016 (2010), arXiv:0911.3535 [astro-ph.HE].
- [57] T. Damour and A. Nagar, Relativistic tidal properties of neutron stars, Phys. Rev. D **80**, 084035 (2009), arXiv:0906.0096 [gr-qc].
- [58] A. J. Penner, N. Andersson, L. Samuelsson, I. Hawke, and D. I. Jones, Tidal deformations of neutron stars: The role of stratification and elasticity, Phys. Rev. D **84**, 103006 (2011), arXiv:1107.0669 [astro-ph.SR].
- [59] J. P. Pereira, M. Bejger, N. Andersson, and F. Gittins, Tidal Deformations of Hybrid Stars with Sharp Phase Transitions and Elastic Crusts, ApJ **895**, 28 (2020), arXiv:2003.10781 [gr-qc].
- [60] F. Gittins, N. Andersson, and J. P. Pereira, Tidal deformations of neutron stars with elastic crusts, Phys. Rev. D **101**, 103025 (2020), arXiv:2003.05449 [astro-ph.HE].
- [61] J. L. Zdunik, M. Fortin, and P. Haensel, Neutron star properties and the equation of state for the core, A&A **599**, A119 (2017).
- [62] K. Chatziioannou, Uncertainty limits on neutron star radius measurements with gravitational waves, arXiv e-prints , arXiv:2108.12368 (2021), arXiv:2108.12368 [gr-qc].
- [63] Z. F. Seidov, The Stability of a Star with a Phase Change in General Relativity Theory, Soviet Ast. **15**, 347 (1971).
- [64] J. L. Zdunik, M. Bejger, P. Haensel, and E.ourgoulhon, Strong first-order phase transition in a rotating neutron star core and the associated energy release, A&A **479**, 515 (2008), arXiv:0707.3691.
- [65] J. Alsing, H. O. Silva, and E. Berti, Evidence for a maximum mass cut-off in the neutron star mass distribution and constraints on the equation of state, MNRAS **478**, 1377 (2018), arXiv:1709.07889 [astro-ph.HE].
- [66] E. Annala, T. Gorda, A. Kurkela, J. Nättilä, and A. Vuorinen, Evidence for quark-matter cores in massive neutron stars, Nature Physics **16**, 907 (2020), arXiv:1903.09121 [astro-ph.HE].
- [67] J. J. Li, A. Sedrakian, and M. Alford, Relativistic hybrid stars with sequential first-order phase transitions and heavy-baryon envelopes, Phys. Rev. D **101**, 063022 (2020).
- [68] B. J. Owen, Maximum elastic deformations of compact stars with exotic equations of state, Phys. Rev. Lett. **95**, 211101 (2005).
- [69] A. Li, Z. Miao, S. Han, and B. Zhang, Constraints on the Maximum Mass of Neutron Stars with a Quark Core from GW170817 and NICER PSR J0030+0451 Data, ApJ **913**, 27 (2021), arXiv:2103.15119 [astro-ph.HE].
- [70] S.-P. Tang, J.-L. Jiang, W.-H. Gao, Y.-Z. Fan, and D.-M. Wei, Constraint on phase transition with the multimessenger data of neutron stars, Phys. Rev. D **103**, 063026 (2021), arXiv:2009.05719 [astro-ph.HE].
- [71] W.-J. Xie and B.-A. Li, Bayesian inference of the dense-matter equation of state encapsulating a first-order hadron-quark phase transition from observables of canonical neutron stars, Phys. Rev. C **103**, 035802 (2021), arXiv:2009.13653 [nucl-th].
- [72] X. Jiménez Forteza, T. Abdelsalhin, P. Pani, and L. Gualtieri, Impact of high-order tidal terms on binary neutron-star waveforms, Phys. Rev. D **98**, 124014 (2018).
- [73] S. K. Greif, K. Hebeler, J. M. Lattimer, C. J. Pethick, and A. Schwenk, Equation of State Constraints from Nuclear Physics, Neutron Star Masses, and Future Moment of Inertia Measurements, ApJ **901**, 155 (2020), arXiv:2005.14164 [astro-ph.HE].
- [74] R. Abbott, T. D. Abbott, S. Abraham, F. Acernese, Ackley, and et al., Gravitational-wave Constraints on the Equatorial Ellipticity of Millisecond Pulsars, ApJ **902**, L21 (2020), arXiv:2007.14251 [astro-ph.HE].
- [75] V. Dergachev and M. A. Papa, Results from high-frequency all-sky search for continuous gravitational waves from small-ellipticity sources, Phys. Rev. D **103**, 063019 (2021), arXiv:2012.04232 [gr-qc].
- [76] R. Abbott, H. Abe, F. Acernese, K. Ackley, N. Adhikari, R. X. Adhikari, and et al., Search for continuous gravitational waves from 20 accreting millisecond X-ray pulsars in O3 LIGO data, arXiv e-prints , arXiv:2109.09255

- (2021), arXiv:2109.09255 [astro-ph.HE].
- [77] R. Abbott, H. Abe, F. Acernese, K. Ackley, N. Adhikari, R. X. Adhikari, and et al., Searches for Gravitational Waves from Known Pulsars at Two Harmonics in the Second and Third LIGO-Virgo Observing Runs, arXiv e-prints , arXiv:2111.13106 (2021), arXiv:2111.13106 [astro-ph.HE].
- [78] A. Bauswein, N.-U. F. Bastian, D. B. Blaschke, K. Chatziioannou, J. A. Clark, T. Fischer, and M. Oertel, Identifying a First-Order Phase Transition in Neutron-Star Mergers through Gravitational Waves, Phys. Rev. Lett. **122**, 061102 (2019), arXiv:1809.01116 [astro-ph.HE].
- [79] S. Blacker, N.-U. F. Bastian, A. Bauswein, D. B. Blaschke, T. Fischer, M. Oertel, T. Sultani, and S. Typel, Constraining the onset density of the hadron-quark phase transition with gravitational-wave observations, Phys. Rev. D **102**, 123023 (2020), arXiv:2006.03789 [astro-ph.HE].